



# Growth and characterizaion of urea *p*-nitrophenol crystal: an organic nonlinear optical material for optoelectronic device application

A. Suresh<sup>1</sup> · N. Manikandan<sup>1</sup> · RO. MU. Jauhar<sup>1,2</sup> · P. Murugakoothan<sup>2</sup> · G. Vinitha<sup>1</sup>

Received: 31 October 2017 / Accepted: 23 March 2018 / Published online: 10 May 2018  
© Springer-Verlag GmbH Germany, part of Springer Nature 2018

## Abstract

Urea *p*-nitrophenol, an organic nonlinear optical crystal was synthesized and grown adopting slow evaporation and seed rotation method. Single crystal X-ray diffraction study confirmed the formation of the desired crystal. High resolution X-ray diffraction study showed the defect nature of the crystal. The presence of functional groups in the material was confirmed by FTIR analysis. UV-Vis-NIR study indicates that the grown crystal has a wider transparency region with the lower cutoff wavelength at 423 nm. The grown crystal is thermally stable up to 120 °C as assessed by TG-DTA analysis. The optical homogeneity of the grown crystal was confirmed by birefringence study. The 1064 nm Nd-YAG laser was used to obtain laser induced surface damage threshold which was found to be 0.38, 0.25 and 0.33 GW/cm<sup>2</sup> for (0 1 0), (1 1 – 1) and (0 1 1) planes, respectively. The dielectric study was performed to find the charge distribution inside the crystal. The hardness property of the titular material has been found using Vicker's microhardness study. The optical nonlinearity obtained from third order nonlinear optical measurements carried out using Z-scan technique showed that these samples could be exploited for optical limiting studies.

## 1 Introduction

Organic nonlinear optical (NLO) materials have attracted much interest due to their properties that has led to widespread applications such as optical switching, optical limiting, optical communication, optical data storage device applications, frequency mixing, laser frequency conversion, optical computing, etc. [1–4]. Organic NLO materials have large second order nonlinearities compared to their counterparts [5]. Organic compounds which possess large  $\pi$ -electron delocalization play a significant function in the area of nonlinear optics. For optical switching and sensor protection applications, the materials which exhibit third-order nonlinear optical (NLO) properties such as nonlinear refraction (NLR) and nonlinear absorption (NLA) are considered to be the ideal candidates [6–8]. In the past few decades, research in identifying new organic NLO materials has gained importance. To understand second order nonlinear optical

property, several trials have been done through hydrogen bonding interactions for the formation of acentric crystal structures. Crystals which possess inversion centers with an additional intermolecular dipole–dipole interaction with close packing, favors third order nonlinear optical limiting and three dimensional fluorescence microscopy applications [9, 10]. Consequently, urea which is a promising organic material exhibiting large nonlinear optical coefficient, high degree of birefringence and relatively high laser damage threshold has been chosen for the present study [11–15]. In literature, even though there are reports on nitrophenol been synthesized with urea to the best of the knowledge of authors, there is no report on its crystalline perfection, fracture mechanics, anisotropic laser damage threshold study, birefringence along with optoelectronic device realization of non-linear optical property of the urea *p*-nitrophenol (UPN) single crystals as optical limiter. Hence, the present work focuses on the above mentioned properties and optical limiting application of urea *p*-nitrophenol single crystal grown by low temperature slow evaporation method.

✉ G. Vinitha  
vinitha.g@vit.ac.in

<sup>1</sup> Division of Physics, School of Advanced Sciences, Vellore Institute of Technology, Chennai 600127, India

<sup>2</sup> MRDL, PG and Research Department of Physics, Pachaiyappa's College, Chennai 600 030, India

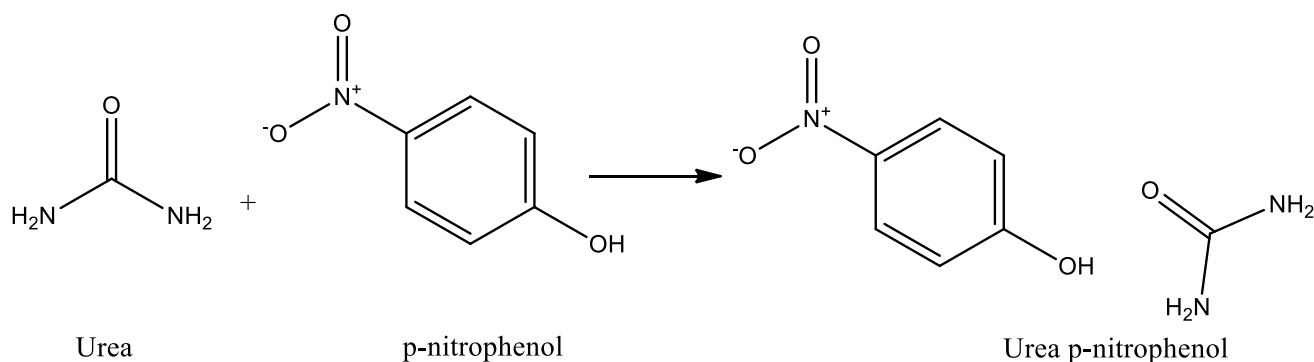


Fig. 1 Reaction scheme of UPN crystal

## 2 Experimental

### 2.1 Material synthesis

Urea and *p*-nitrophenol have been used as precursors for the synthesis of UPN crystal. Methanol, used as solvent resulted in a definite morphology as compared to other solvents as reported in literature [14, 15]. The solution was stirred for 4 h to attain homogeneity. The resulting solution was filtered using whatman filter paper and perforated polythene sheet was used to cover the solution in beaker to hinder abundant evaporation. The filtered solution was allowed to evaporate at room temperature. After a span of 15 days, small seed crystals were found in the solution. The reaction scheme of UPN is shown in Fig. 1.

The obtained seed crystals were collected, ground and used for solubility study. The solubility study was performed with concentration as a function of temperature in 5 °C intervals from 35 to 50 °C using a constant temperature water bath with temperature accuracy of  $\pm 0.01$  °C by gravimetric method. The positive solubility gradient of UPN in methanol solvent is obtained from the solubility curve and is depicted in Fig. 2. At 40 °C, the solubility limit of UPN is estimated as 62.7 g/100 mL. The constant temperature water bath was maintained at 40 °C and the prepared UPN solution was placed inside it based on the solubility data. Bulk crystal of UPN was obtained after a period of 20 days with dimensions  $25 \times 7 \times 8$  mm<sup>3</sup> and is shown in Fig. 3.

## 3 Results and discussion

### 3.1 Single crystal X-ray diffraction and morphology studies

Bruker axs SMART APEXII single crystal X-ray diffractometer equipped with graphite monochromatic MoK $\alpha$  ( $\lambda = 0.71073$  Å) radiation and CCD detector was used to

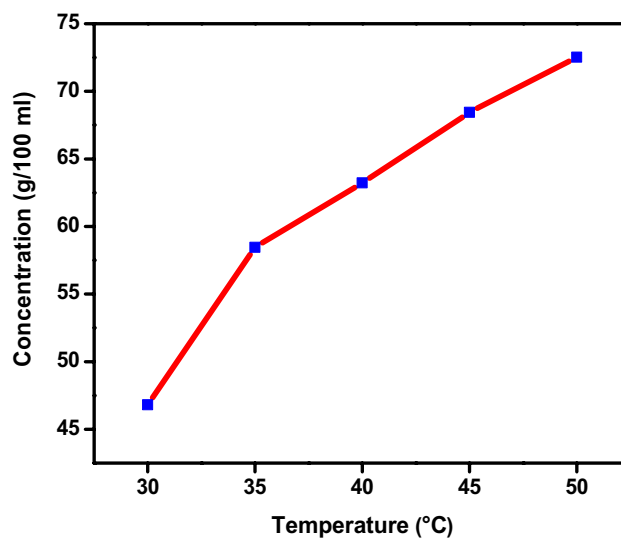


Fig. 2 Solubility curve of UPN in methanol solvent

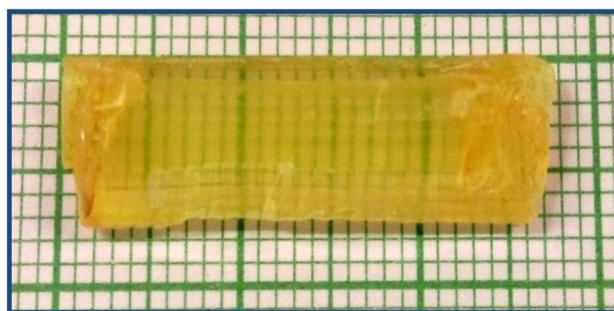


Fig. 3 Photograph of UPN crystal

collect X-ray diffraction intensity data at room temperature (293 K). A crystal of dimensions  $0.30 \times 0.25 \times 0.15$  mm<sup>3</sup> was fixed on a glass fiber using cyanoacrylate adhesive. The method of difference vectors was used to determine

the unit cell parameters from 36 frames measured ( $0.5^\circ$  phi-scan) from three different crystallographic zones.

The geometrical positions of the N- and C-bound H atoms are ( $N-H=0.86 \text{ \AA}$ ,  $C-H=0.93-0.97 \text{ \AA}$ ) which were allowed to ride on their parent atoms, with  $U_{iso}(H)=1.2U_{eq}(N,C)$ .

The UPN crystal belongs to triclinic crystal system with space group  $P\bar{1}$ . The observed lattice parameter values are  $a=3.7461(3) \text{ \AA}$ ,  $b=10.1888(9) \text{ \AA}$  and  $c=11.7575(9) \text{ \AA}$ ,  $\alpha=98.67^\circ$ ,  $\beta=92.41^\circ$ ,  $\gamma=99.34^\circ$  and volume  $V=436.73(6) \text{ \AA}^3$ . In the crystal structure of the title compound,  $C_6H_5N_1O_3 \cdot C_1H_6N_2O_1$ , the dihedral angle between the benzene ring and urea mean plane ( $N2/C7/O4/N3$ ) is  $34.08(16)^\circ$ . The nitrophenol moiety is essentially planar with maximum deviation of  $-0.0040 \text{ \AA}$  for the N1 atom. In the crystal, molecules are linked via  $N-H\cdots O$  and  $O-H\cdots O$ , bifurcated hydrogen bonds forming inversion dimers with  $R_2^2(8)$  and  $R_2^1(6)$  ring motif in a two dimensional network lying parallel to (010). The crystal packing is further stabilized by  $\pi-\pi$  stacking interactions. The crystal packing of UPN crystal is shown in Fig. 4. The morphology of the UPN crystal was generated using WINXMORPH software and is shown in Fig. 5.

### 3.2 High resolution X-ray diffraction study

Multicrystal X-ray diffractometer with  $MoK\alpha_1$  radiation was used to perform the High resolution X-ray diffraction technique [16]. The (0 1 0) lattice plane was selected for HRXRD, the UPN crystal was chemically etched in a

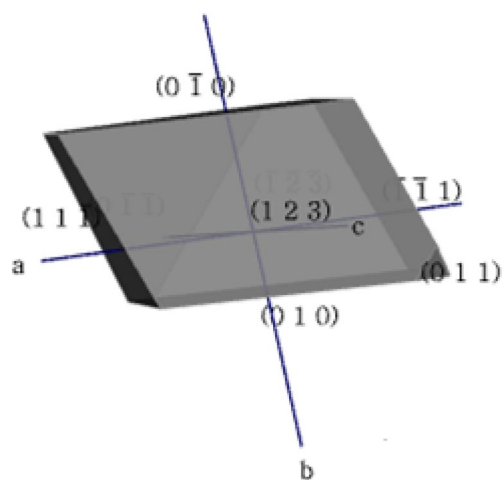


Fig. 5 Morphology of UPN crystal

non-preferential etchant of acetone before recording the diffraction curve, the recorded diffraction curve is shown in Fig. 6. Notably a single peak in the diffraction curve clearly shows that there are no structural grain boundaries observed in the UPN crystal. This indicates that the possibility of impurities at macroscopic level is very less. For an ideally perfect crystal, the plane wave theory of dynamical x-ray diffraction [17] is used to calculate the full width at half maximum (FWHM). The FWHM of the UPN crystal is found to be 13 arc s, which is higher than that of the expected value.

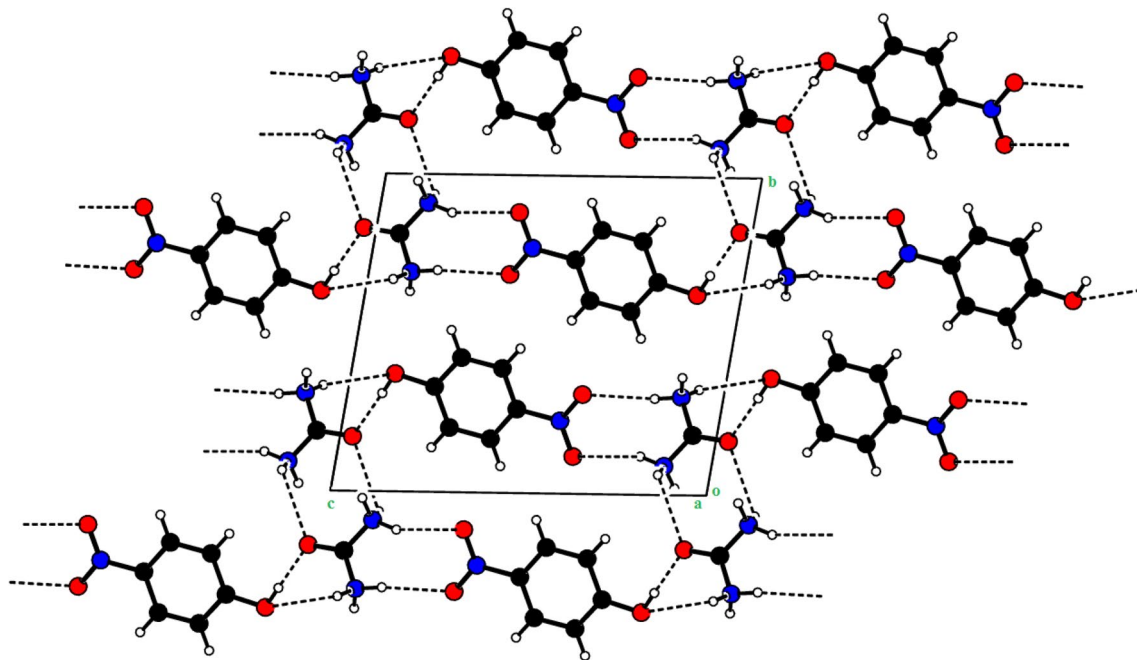


Fig. 4 Packing diagram of UPN crystal

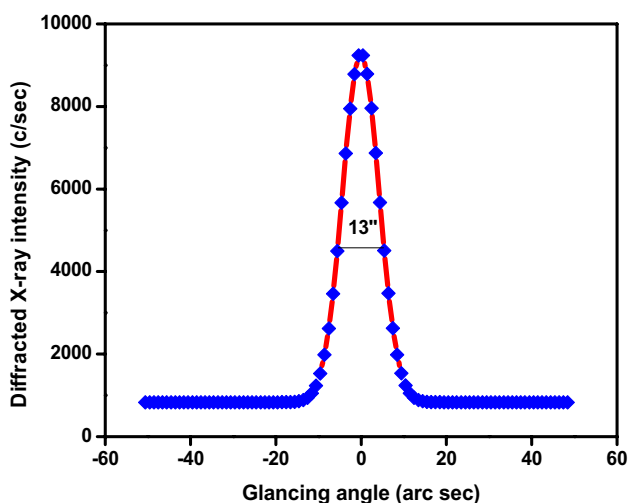


Fig. 6 HRXRD curve of UPN crystal

### 3.3 FTIR analysis

The Fourier Transform Infrared (FTIR) spectrum of UPN crystal was carried out using KBr pellet technique ranging from 400 to 4000  $\text{cm}^{-1}$ . The recorded spectrum is shown in Fig. 7. From the spectrum, C=C asymmetric stretching vibration is observed around 1639  $\text{cm}^{-1}$ , the asymmetric stretching vibrations at 1580  $\text{cm}^{-1}$  is attributed towards the presence of aromatic  $\text{NO}_2$  of the *p*-nitrophenol [14],  $\text{NH}_3^+$  bending vibration at 1488  $\text{cm}^{-1}$ , C–H in plane and out-of-plane bending vibrations at 1337 and 846  $\text{cm}^{-1}$ , respectively, in-plane-bending having sharp and strong intensity bands at 1337  $\text{cm}^{-1}$ , CH wagging at 1154  $\text{cm}^{-1}$ , C–C–N asymmetric bending vibrations at the region of 1108  $\text{cm}^{-1}$  and  $\text{COO}^-$  bending vibration at the region of 609  $\text{cm}^{-1}$  [11].

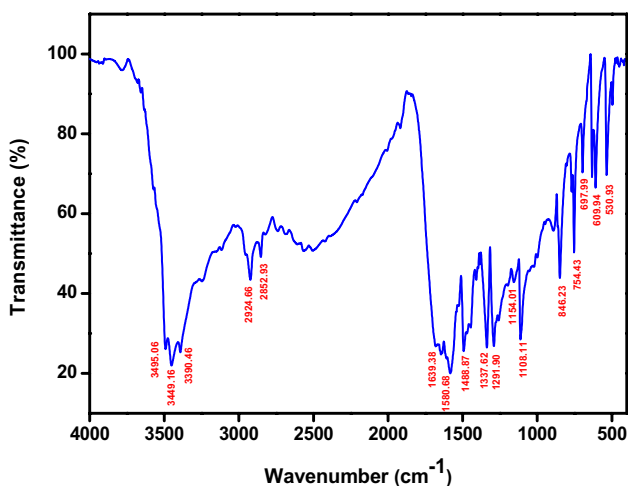


Fig. 7 FTIR spectrum of UPN crystal

The spectrum of  $\text{C}\equiv\text{H}$  symmetrical band was observed at 3390  $\text{cm}^{-1}$  and also the absorption peak was confirmed to be  $\text{COO}^-$  stretching vibration. The wave number of 697  $\text{cm}^{-1}$  observed as sharp intense peak is confirmed to be C=O bending vibration of the urea group [5]. The C–H asymmetric stretching vibration corresponds to the peak at 2852  $\text{cm}^{-1}$  [18]. The peaks at 3495 and 1291  $\text{cm}^{-1}$  are assigned to be symmetric  $\text{NH}_2$  stretching vibration and CH stretching vibration, respectively [19]. The  $\text{NO}_2$  scissoring occurred at 530  $\text{cm}^{-1}$  [3]. The peaks at 3449 and 2924  $\text{cm}^{-1}$  correspond to the asymmetric stretching vibrations of  $\text{NH}_2$  and C–H superimposed upon O–H stretching vibrations [20]. Around the region of 754  $\text{cm}^{-1}$ ,  $\text{NH}_2$  rocking vibrations takes place. All the observations clearly indicate the presence of urea *p*-nitrophenol in the crystal lattice [21]. The peak assignments for various functional groups are given in Table 1.

### 3.4 Optical transmittance study

Optical transmittance study was performed in the range of 200–900 nm using Thermoscientific-Evolution 300 UV-Vis-NIR Spectrophotometer. Figure 8 depicts the UV-Vis-NIR spectrum of UPN crystal. As seen from the figure, the transparency of the UPN crystal is good in the visible and IR region with lower cut-off wavelength at 423 nm. The region between 450 and 800 nm shows that there is no absorption which indicates that the UPN crystal would be a potential candidate for optical applications.

Table 1 Vibrational assignments of UPN crystal

Wavenumber ( $\text{cm}^{-1}$ )	Assignments
3495	$\text{NH}_2$ symmetric stretching
3449	Asymmetric stretching of $\text{NH}_2$
3390	$\text{C}\equiv\text{H}$ symmetrical band stretching
2924	C–H stretching superimposed upon O–H stretching
2852	C–H asymmetric stretching
1639	C=C asymmetric stretching
1580	$\text{COO}^-$ asymmetric stretching
1488	$\text{NH}_3^+$ bending
1337	CH in-plane bending
1291	CH stretching vibration
1154	CH wagging
1108	C–C–N asymmetric bending
846	C–H out-of-plane bending
754	$\text{NH}_2$ rocking
697	C=O stretching
609	$\text{COO}^-$ bending
530	$\text{NO}_2$ scissoring

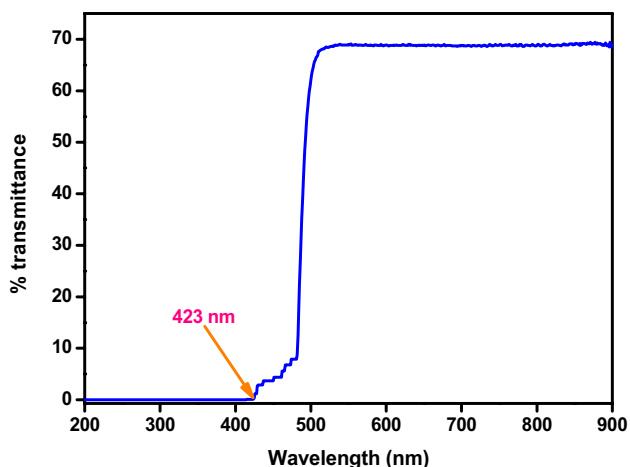


Fig. 8 Optical transmittance of UPN crystal

The optical absorption coefficient ( $\alpha$ ) is evaluated using the relation.

$$\alpha = \frac{2.3026}{t} \log(1/T), \tag{1}$$

where ‘ $T$ ’ the transmittance and ‘ $t$ ’, the sample thickness.

The transmission spectrum was used to calculate the band gap and the absorption edge was used to evaluate the optical absorption coefficient ( $\alpha$ ) using the relation [18].

$$(\alpha h\nu)^2 = A(E_g - h\nu), \tag{2}$$

where  $E_g$  is the optical band gap of the crystal and  $A$  is a constant. A plot between the variation of  $(\alpha h\nu)^2$  with  $(h\nu)$  in the fundamental absorption region [11] is depicted in Fig. 9. By extrapolating the linear part of the graph, the band gap of the crystal was found to be 2.55 eV.

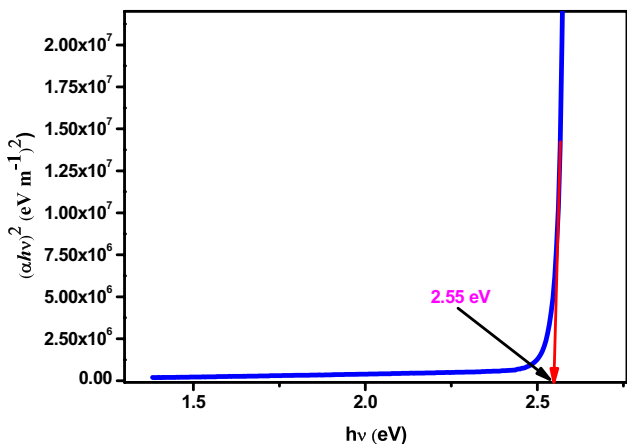


Fig. 9 Plot of photon energy vs  $(\alpha h\nu)^2$  of UPN crystal

### 3.5 Thermal study

The TG-DTA analysis of UPN material was carried out by SII TG/DTA7200, EXSTAR in the temperature range 30–650 °C under nitrogen atmosphere. The sample weighing 3.2 mg was taken for the analysis and the thermogram obtained is shown in Fig. 10. The TG curve clearly shows that the UPN crystal is stable till 120 °C and free from moisture. The TG curve shows that as the material was heated from 30 to 650 °C, there are two levels of weight loss pattern. A major weight loss of the title compound was observed in the temperature range 120–500 °C which is about 65%. In the temperature range between 501 and 600 °C, there is a second stage of weight loss which is about 33%. The melting point of the UPN crystal was cross checked using a homemade melting point apparatus. The removal of materials into gaseous products takes place when the decomposition occurs around 650 °C [22]. Thus, it was concluded from TG-DTA curve that below 120 °C the UPN crystal could be exploited for applications.

### 3.6 Birefringence study

The birefringence study was carried out on a well-polished UPN crystal having thickness of 1.94 mm using a channel spectrum. Light from a 1000 W tungsten halogen lamp was allowed to fall on the UPN crystal provided the crystal is placed in between analyzer and polarizer. When the transmitted light passes through the analyzer, it produces a fringe pattern. The birefringence values can be calculated using the formula.

$$\Delta n = \frac{k\lambda}{t}, \tag{3}$$

where,  $k$  is the fringe order,  $t$  is thickness of the crystal and  $\lambda$  is the wavelength of the source. A graph between wavelength and birefringence is shown in Fig. 11. The graph clearly

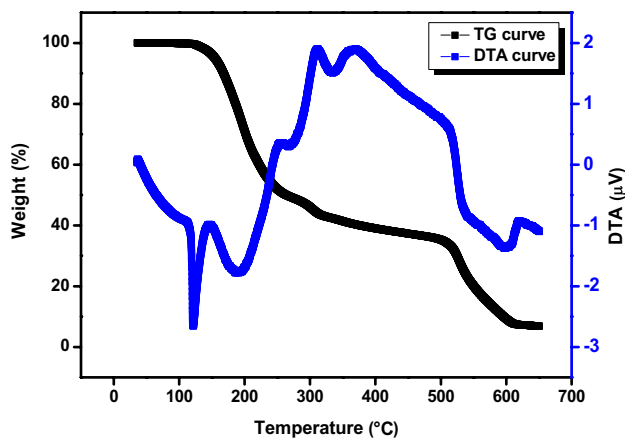
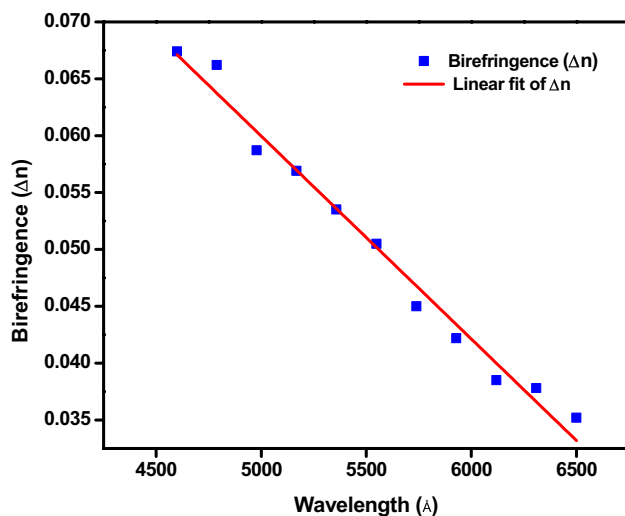


Fig. 10 TGA and DTA curve of UPN crystal



**Fig. 11** Plot of wavelength versus birefringence of UPN crystal

shows that there is a decrease in the value of birefringence when the wavelength increases. From this measurement, it is observed that the UPN crystal possesses good birefringence values in the visible wavelength region between 0.196 and 0.160 in the wavelength region ranging between 450 and 650 nm. The low birefringence value [17] in the said wavelength region indicates that the UPN crystal is an ideal candidate for nonlinear optical applications. The birefringence values of the grown crystal as compared with some other NLO crystals are tabulated in Table 2.

### 3.7 Laser damage threshold study

Laser induced surface damage threshold (LDT) study is one of the most important parameters for materials to be employed in NLO applications. A number of laser parameters which include the location of the beam, beam size, longitudinal and transverse mode structures, pulse

**Table 2** Comparative study of birefringence value of UPN crystal with some other NLO crystals

Crystal	Birefringence value
Sodium sulfanilate dehydrate	0.0260 <sup>a</sup>
Benzophenone	0.0235 <sup>b</sup>
L-Arginine acetate	0.04325 <sup>c</sup>
Urea tartaric acid	0.0736 <sup>d</sup>
Urea <i>p</i> -nitrophenol (UPN)	0.0535 <sup>e*</sup>

<sup>a</sup>Ref. [23]

<sup>b</sup>Ref. [24]

<sup>c</sup>Ref. [25]

<sup>d</sup>Ref. [18]

<sup>e\*</sup>Present work

duration, energy, wavelength, etc determine the laser damage threshold [18]. A Q-switched Nd:YAG laser in TEM<sub>00</sub> mode was operated with wavelength 532 nm and a pulse width of 30 ns. A repetition rate of 5 Hz was used as the source for determining the LDT value of the UPN crystal. The rate of thermal condition controls the laser induced damage threshold along with the atomic lattice in the long range pulse at ( $\tau > 100$  ps) and the optical breakdown with the nonlinear ionization mechanism becomes a short range pulse at ( $\tau < 100$  ps). Plano convex lens of focal length 30 cm was used to focus the laser beam of 1 mm diameter on the UPN crystal. The energy of the laser pulses with a half wave plate of the polarizer was used to vary the attenuator. The pulse energy of each shot was measured using a phototube along with an oscilloscope. The surface damage threshold can be evaluated using the relation.

$$\text{Power density } (P_d) = E / \tau \pi r^2 \quad \text{W/cm}^2, \quad (4)$$

where  $r$  is the radius of the spot (mm),  $\tau$  is the pulse width (ns), and  $E$  is the energy (mJ). The laser induced damage threshold of the UPN crystal was found to be 0.38, 0.25 and 0.33 GW/cm<sup>2</sup> for planes (0 1 0), (1 1 - 1) and (0 1 1), respectively. A slightly higher LDT value along (0 1 0) plane compared with other two planes indicates the defect density along (0 1 0) plane to be lower. This implies that LDT of a sample is much more influenced by its defect state. The LDT value of UPN crystal is compared with well-known crystals and has been tabulated in Table 3.

### 3.8 Dielectric analysis

Dielectric behavior of the grown UPN crystal was studied using PSM 1735 LCR meter impedance analyzer. Dielectric study is an important phenomenon to study the detailed information about the nature of the atoms, ions

**Table 3** Comparative study of laser damage threshold value of UPN crystals with some organic and inorganic NLO crystals

Crystal	Laser damage threshold (GW/cm <sup>2</sup> )
Potassium dihydrogen phosphate (KDP)	0.20 <sup>a</sup>
Urea	1.50 <sup>a</sup>
Benzimidazole	1.71 <sup>a</sup>
Beta-barium borate (BBO)	5.0 <sup>a</sup>
L-arginine phosphate (LAP)	10.0 <sup>a</sup>
Urea <i>p</i> -nitrophenol (UPN)	
(0 1 0)	0.38 <sup>b*</sup>
(1 1 - 1)	0.25 <sup>b*</sup>
(0 1 1)	0.33 <sup>b*</sup>

<sup>a</sup>Ref. [26]

<sup>b\*</sup>Present work

and the bonding polarization mechanism of the grown crystals [27]. The grown UPN crystal with thickness 1 mm was coated with silver paste on both sides of the crystal as like a parallel plate capacitor to ensure good electrical conductivity. The dielectric constant of the grown crystal is obtained from the following relation.

$$\epsilon_r = \frac{Cd}{\epsilon_0 A}, \tag{5}$$

where  $\epsilon_0$  is the permittivity of the free space,  $A$  is the area of the crystal,  $d$  is the thickness of the grown crystal and  $C$  is the capacitance. The dielectric loss value of the grown crystal was calculated using the relation.

$$\epsilon'' = \epsilon_r D'', \tag{6}$$

where  $D$  is the dissipation factor. The dielectric constant and dielectric loss of the grown UPN crystal are shown in Figs. 12 and 13, respectively. As seen in the figures, dielectric constant ( $\epsilon_r$ ) and dielectric loss ( $D$ ) gradually decrease when frequency increases. This may be due to the presence of all four polarizations namely, orientation, space charge, electronic and ionic polarization. The low dielectric loss in the high frequency range suggests that the UPN crystal possesses enhanced optical quality with lesser defects.

### 3.9 Microhardness study

Vicker’s microhardness study was performed to find the mechanical properties of UPN crystal with different loads ranging from 25 to 100 g for varying indentations. The time of indentation was kept uniformly at 10 s for different loads using Economet microhardness tester fitted with a diamond pyramidal indenter fixed to an optical microscope.

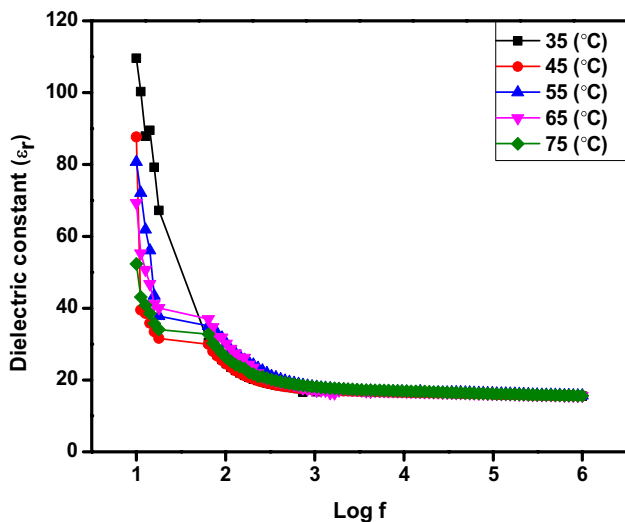


Fig. 12 Plot of  $\log f$  versus dielectric constant of UPN crystal

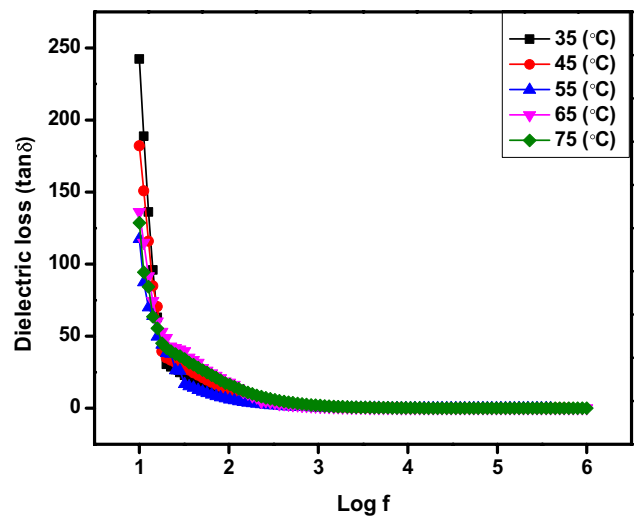


Fig. 13 Plot of  $\log f$  versus dielectric loss

The difference in the value of microhardness ( $H_v$ ) for corresponding loads ( $P$ ) is shown in Fig. 14. The hardness number ( $H_v$ ) was evaluated using the relation.

$$H_v = 1.8544 P/d^2 \text{ (kg/mm}^2\text{)}, \tag{7}$$

where  $H_v$  is the Vicker’s hardness number,  $d$  is the applied load in kg and  $P$  is the diagonal length of the impression in mm. From the figure, it is noted that as there is an increase in applied load there is an increase in the hardness number. This effect is known as the reverse indentation size effect (RISE) [28]. It clearly indicates that under the condition that if  $n > 2$ , as the value of  $P$  increases, there is an increase in the value of  $H_v$  and when  $n < 2$ , the value of  $P$  decreases with increase of load. This condition matches well with the experimental data and thereby it confirms the reverse indentation size effect. It was found that for hard materials, the

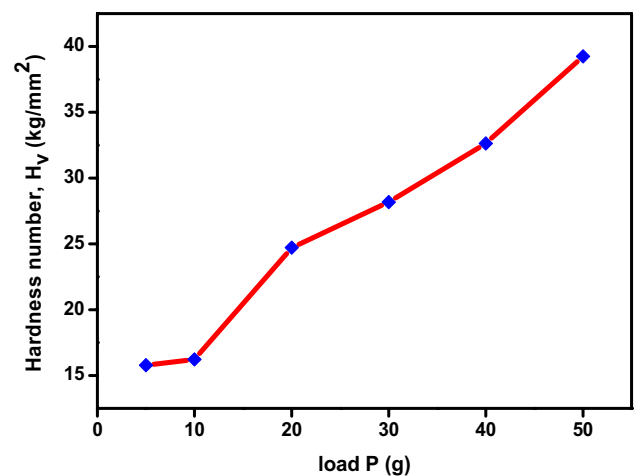


Fig. 14 Load ( $P$ ) versus Hardness number ( $H_v$ ) of UPN crystal

work hardening coefficient ( $n$ ) lies between 1 and 1.6 and for soft materials, the work hardening coefficient ( $n$ ) lies above 1.6 [29].

The hardness coefficient of the UPN crystal was found by applying the Mayer’s relation,

$$P = kd^n, \tag{8}$$

where ‘ $n$ ’ is the Mayer’s index and  $k$  is the materials constant. The work hardening coefficient ( $n$ ) depicted in Fig. 15, is obtained from the slope of  $\log d$  versus  $\log P$  and the value is found to be 2.12. Thus, the UPN crystal belongs to the soft-material category.

The yield strength ( $\sigma_y$ ) of the title compound was determined using the relation,

$$\sigma_y = (H_v/3). \tag{9}$$

The Wooster’s empirical formula  $C_{11} = H^{7/4}$  was used to calculate the elastic stiffness constant ( $C_{11}$ ) for varying loads, to get a clear idea regarding the tightness of bonding between neighboring atoms. The load dependent parameters such as  $H_v$ ,  $n$ , yield strength ( $\sigma_y$ ), and elastic stiffness constant ( $C_{11}$ ) are presented in Table 4.

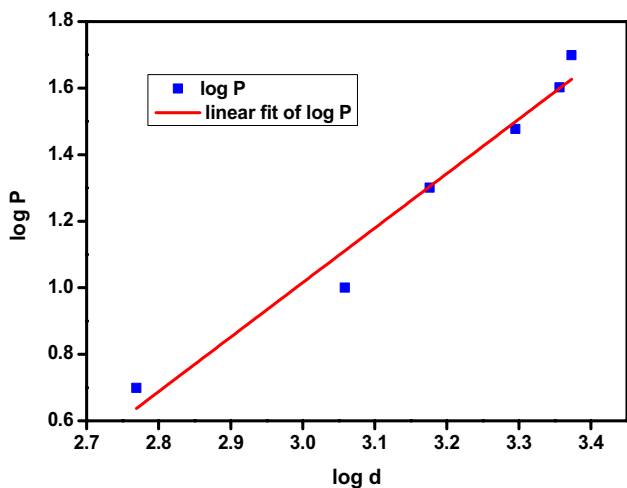


Fig. 15  $\log d$  versus  $\log P$  of UPN crystal

**Table 4** The Vicker’s hardness ( $H_v$ ), yield strength ( $\sigma_y$ ) and elastic stiffness constant ( $C_{11}$ ) for different loads of UPN crystal

$P$ (g)	$H_v$	$\sigma_y$ (kg/mm <sup>2</sup> )	$C_{11} \times 10^{14}$ (Pa)
10	24	8	2.60237
25	36	12	5.29089
45	48	16	8.75330
50	56	18.6	11.46381
100	22	7.33	2.33480

### 3.10 Z-scan study

To determine nonlinear absorption coefficient,  $\beta$  and nonlinear index of refraction,  $n_2$  the Z-scan technique was used [30]. Nonlinear refractive index is proportional to the real part of the third-order susceptibility, [ $\text{Re}\chi^{(3)}$ ] and the nonlinear absorption coefficient is proportional to the imaginary part of the third order susceptibility, [ $\text{Im}\chi^{(3)}$ ].

A 532 nm diode pumped CW Nd:YAG Laser (Coherent Compass™215M-50) was used to perform the Z-scan experiments. A 3.5 cm focal length lens was used to focus the laser. The laser beam waist at the point of focus is calculated to be 15.84  $\mu\text{m}$  and the Rayleigh length is found to be 1.48 mm.

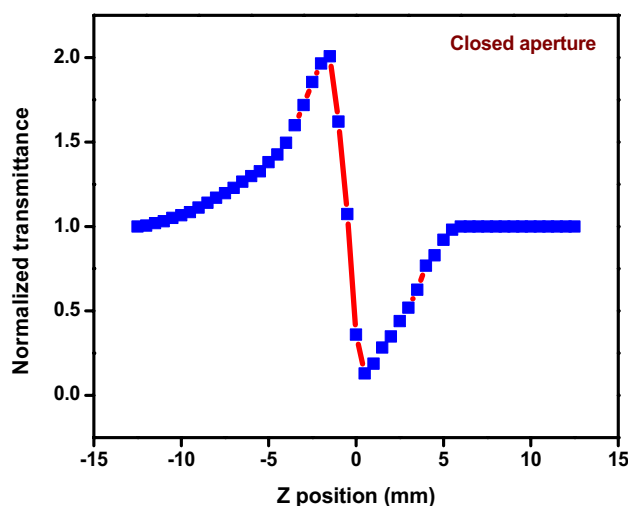


Fig. 16 Closed aperture curve of UPN crystal

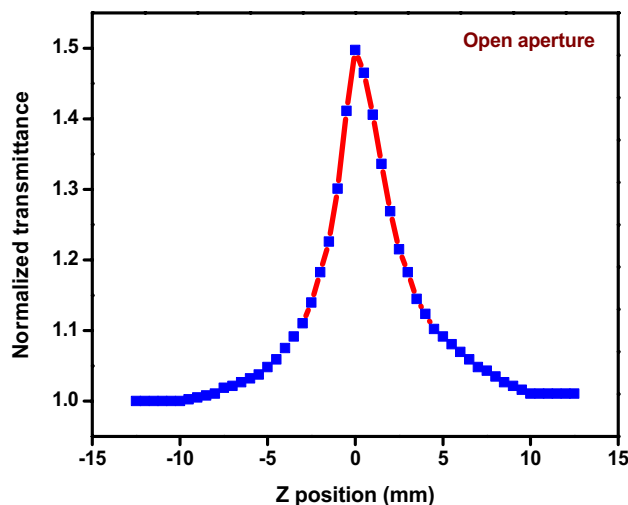


Fig. 17 Open aperture curve of UPN crystal



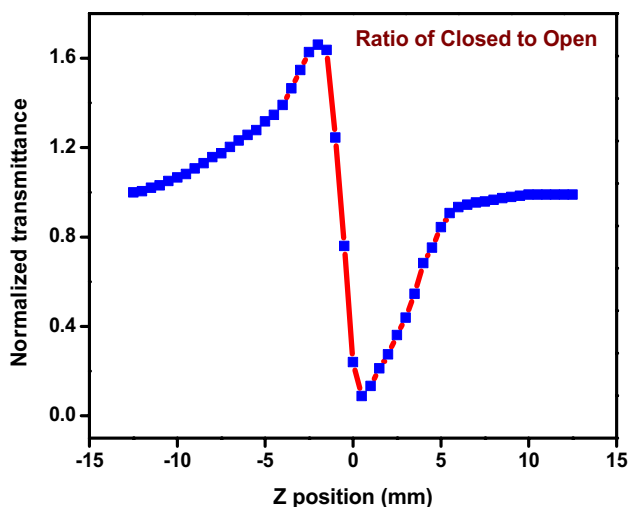


Fig. 18 Ratio of closed to open aperture curve of UPN crystal

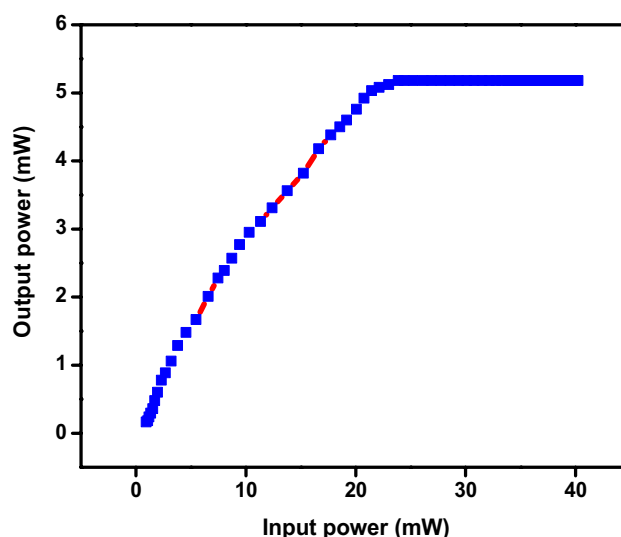


Fig. 19 Optical limiting curve of UPN crystal

Table 5 Observed nonlinear optical parameter for grown UPN crystal

$n_2 \times 10^{-8}$ ( $\text{cm}^2/\text{W}$ )	$\beta \times 10^{-4}$ ( $\text{cm}/\text{W}$ )	$\text{Re } \chi^{(3)} \times 10^{-6}$ (esu)	$\text{Im } \chi^{(3)} \times 10^{-6}$ (esu)	$\chi^{(3)} \times 10^{-6}$ (esu)
7.85	0.35	3.95	2.17	4.51

The UPN crystal was translated across the focal region along the direction of the propagation laser beam i.e, the axial direction. The aperture which is kept at a far field with the help of the photodetector connected to the digital power meter (Field master GS-coherent) was used to measure the transmission beam coming out of the sample. For an open aperture Z-scan, the entire laser beam transmitted through the sample was collected by means of a lens which replaces the aperture.

The graph for closed, open and ratio of the closed-to-open normalized Z-scan UPN crystal is depicted in Figs. 16, 17 and 18. The closed aperture Z-scan shows that a peak followed by a valley-normalized transmittance is obtained

which shows the sign of nonlinear refraction to be negative, i.e., self-defocusing. Local variations in the refractive index with respect to temperature lead to self-defocusing [31]. The calculations were carried out using standard equations [32] and the nonlinear parameters of UPN as tabulated in Table 5. The Comparison of nonlinear refractive index ( $n_2$ ) nonlinear absorption coefficient ( $\beta$ ) and third order nonlinear optical susceptibility [ $\chi^{(3)}$ ] with parent material are tabulated in Table 6.

### 3.11 Optical limiting study

The nonlinearity exhibited by the UPN crystal has been exploited for devising optical limiter. The experimental setup for optical limiting is very similar to the standard Z-scan. To vary the input power, an additional polarizer-analyzer combination (PA) was used. With the incident input intensity at very low values, the transmitted output intensity varies linearly and reaches a plateau and gets saturated when there is an increase in the input power, at a point defined as the

Table 6 Comparison of nonlinear refractive index ( $n_2$ ), nonlinear absorption coefficient ( $\beta$ ) and third order nonlinear optical susceptibility [ $\chi^{(3)}$ ] with parent materials and some other organic crystals

Name of the crystal	$n_2$ ( $\text{cm}^2/\text{W}$ )	$\beta$ ( $\text{cm}/\text{W}$ )	$\chi^{(3)}$ (esu)	References
Isonicotinamide <i>p</i> -nitrophenol (ICPNP)	$8.11 \times 10^{-8}$	$0.09 \times 10^{-4}$	$5.03 \times 10^{-6}$	[33]
Tri-nitrophenol methyl <i>p</i> -hydroxybenzoate (TNMPHB)	$-3.45 \times 10^{-8}$	$-2.05 \times 10^{-4}$	$1.546 \times 10^{-6}$	[34]
2-Amino-4-picolinium toluene sulfonate (2A4PTS)	$-6.8 \times 10^{-8}$	$-7.7 \times 10^{-4}$	$3.38 \times 10^{-6}$	[35]
Cyclohexylammonium acetate (CYHAC)	$-4.920 \times 10^{-8}$	$0.080 \times 10^{-4}$	$2.394 \times 10^{-6}$	[36]
8-Hydroxyquinolinium 2-chloro-5-nitrobenzoate dihydrate (8HQ2C5N)	$7.23 \times 10^{-8}$	$2.04 \times 10^{-4}$	$3.51 \times 10^{-10}$	[37]
Urea <i>p</i> -nitrophenol (UPN)	$7.85 \times 10^{-8}$	$0.35 \times 10^{-4}$	$4.51 \times 10^{-6}$	Present work

limiting amplitude [38]. Figure 19 illustrates the optical limiting curve of UPN crystal.

## 4 Conclusions

UPN, an organic single crystal was grown by the low temperature slow evaporation technique. The crystalline perfection of UPN was investigated by high resolution X-ray diffraction analysis. From the analysis it is evident that no structural grain boundaries have been found in the grown crystal. The UPN crystal is transparent in the whole of visible region which is confirmed from the UV–Vis spectral studies. Material is found to be stable up to 120 °C as observed from the TG-DTA curve. The laser damage threshold study confirms the anisotropic nature of the grown UPN crystal. The dielectric studies reveal that the UPN crystal exhibits normal dielectric behavior. The UPN crystal belongs to the soft material category as found from the microhardness studies. The UPN material has defocusing nature with a negative nonlinear absorption coefficient which was found out from Z-scan technique. Nonlinear characteristics and optical limiting studies show UPN crystal to be potential candidate for optoelectronic device fabrication.

**Acknowledgements** The authors gratefully acknowledge Department of Atomic Energy Board of Research in Nuclear Sciences (DAE-BRNS), Government of India for their support by funding this Research work (Sanction Number: 34/14/55/2014-BRNS).

## References

1. V. Chithambaram, S. Jerome Das, R. ArivudaiNambi, S. Krishnan, *Solid State Sci.* **14**, 216–218 (2012)
2. M. Silambarasan, A. Krishna Kumar, I. Thirunavukkarasu, R. Md Zahid, P.R. Mohan Kumar, Umarani, *Spectrochim. Acta Part A* **142**, 101–109 (2015)
3. C. Shanthi, P. Krishnan, Selvarajan, *J. Cryst. Growth* **393**, 7–12 (2014)
4. T. Prasanyaa, V. Jayaramakrishnan, M. Haris, *Optik* **125**, 732–736 (2014)
5. V. Chithambaram, S. Krishnan, *Opt. Laser Tech.* **55**, 18–20 (2014)
6. D.S. Chemla, J. Zyss, *Quantum Electronics Principles and Applications Series eds.* (Academic Press, Orlando, FL, 1985)
7. X. Xu, W. Qiu, Q. Zhou, J. Tang, F. Yang, Z. Sun, P. Audebert, *J. Phys. Chem. B* **112**, 4913–4917 (2008)
8. J. Xu, J. Chen, L. Chen, R. Hu, S. Wang, S. Li, J.S. Ma, G. Yang, *Dyes Pigm.* **109**, 144 (2014)
9. P.J. Fagan, M.D. Ward, J.C. Calabrese, *J. Am. Chem. Soc.* **111**, 1698 (1989)
10. RO.MU. Jauhar, S. Kalainathan, P. Murugakoothan, *J. Cryst. Growth* **424**, 42–48 (2015)
11. R. Rathika, Ganapathi, Raman, *Optik* **125**, 2978–2982 (2014)
12. K. Sunil Verma, S. Ramachandra Rao, K.S. Kar, Bartwal, *Spectrochim. Acta Part A* **153**, 16–21 (2016)
13. T. Uma Devi, N. Lawrence, R. Ramesh Babu, S. Selvanayagam, H. Stoeckli-Evans, K. Ramamurthi, *J. Cryst. Growth* **311**, 3485–3490 (2009)
14. M. Krishna Mohan, S. Ponnusamy, C. Muthamizhchelvan, *Mater. Chem. Phys.* **195**, 224–228 (2017)
15. S. Selvakumar, A. Leo Rajesh, *J. Mater. Sci. Mater. Electron.* **27**, 7509–7517 (2016)
16. G. Peramaiyan, P. Pandi, N. Vijayan, G. Bhagavannarayana, R. Mohan Kumar, *J. Cryst. Growth* **375**, 6–9 (2013)
17. P. Vinothkumar, R. Mohan Kumar, R. Jayavel, A. Bhaskaran, *Opt. Laser Technol.* **81**, 145–152 (2016)
18. P. Vinothkumar, K. Rajeswari, R. Mohan Kumar, A. Bhaskaran, *Spectrochim. Acta Part A* **145**, 33–39 (2015)
19. K. Sathishkumar, J. Chandresekaran, Y. Matsushita, A. Sato, C.I. Sathish, K. Yamaura, B. Babu, *Optik* **126**, 981–984 (2015)
20. B.K. Singh, N. Sinha, N. Singh, K. Kumar, M.K. Gupta, B. Kumar, *J. Phys. Chem. Solids* **71**, 1774–1779 (2010)
21. M.R. Jagadeesh, H.M. Suresh Kumar, R. Ananda, Kumari, *Optik* **126**, 4014–4018 (2015)
22. RO.MU. Jauhar, V. Viswanathan, P. Vivek, G. Vinitha, D. Velmurugan, P. Murugakoothan, *RSC Adv.* **6**, 57977 (2016)
23. M. Senthil Pandian, P. Ramasamy, *Mater. Chem. Phys.* **132**, 1019–1028 (2012)
24. M. Senthil Pandian, K. Boopathi, P. Ramasamy, G. Bhagavannarayana, *Mater. Res. Bull.* **47**, 826–835 (2012)
25. N. Renuka, N. Vijayan, R. BrijeshRathi, K. Ramesh Babu, D. Nagarajan, G. Haranath, Bhagavannarayana, *Optik* **123**, 189–192 (2012)
26. N. Vijayan, G. Bhagavannarayana, T. Kanagasekaran, R. Ramesh Babu, R. Gopalakrishnan, P. Ramasamy, *Cryst. Res. Technol.* **41**(8), 784–789 (2006)
27. M. Manivannan, S.A. Martin, M. BrittoDhas, Jose, *J. Cryst. Growth* **455**, 161–167 (2016)
28. K. Sangwal, *Mater. Chem. Phys.* **63**, 145–152 (2000)
29. E.M. Onitsch, *Mikroskopie* **2** (1947) 131
30. M. Sheik-bahae, A.L.I.A. Said, T. Wei, *IEEE J. Quant. Electron.* **26**, 760–769 (1990)
31. T.D. Krauss, F.W. Wise, *Appl. Phys. Lett.* **65**, 1739 (1994)
32. T. Cassano, R. Tommasi, M. Ferrara, F. Babudri, G.M. Farinola, F. Naso, *Chem. Phys.* **272**, 111–118 (2001)
33. B. Vijayalakshmi, G. Vidyavathy, Vinitha, *J. Cryst. Growth* **448**, 82–88 (2016)
34. C. Vesta, R. Uthrakumar, G. Vinitha, J. Ramalingam, S.J. Das, *J. Cryst. Growth* **311**, 4016–4021 (2009)
35. G. Anandhababu, P. Ramasamy, *Spectrochim. Acta Part A* **82**, 521–526 (2011)
36. R. Gomathi, S. Madeswaran, D. RajanBabu, G. Aravindan, *Mater. Lett.* **209**, 240–243 (2017)
37. M. DivyaBharathi, G. Ahila, J. Mohana, G. Chakkaravarthi, G. Anbalagan, *Mater. Chem. Phys.* **192**, 215–227 (2017)
38. C. Babeela, T.C. Sabari Girisun, G. Vinitha, *J. Phys. D Appl. Phys.* **48**, 065102–065109 (2015)